DOI:10. 11973/jxgccl240361

TIG 熔修距离和电流对 Q690D 钢 GMAW 十字接头疲劳性能的影响

白海明[1],李子豪[2],马一鸣[2],安洪亮[2]
(1. 郑州煤矿机械集团股份有限公司,郑州 450016;2. 中国机械总院集团哈尔滨焊接研究所有限公司,哈尔滨 150028)

摘　要: 对Q690D低合金高强钢熔化极气体保护电弧焊(GMAW)十字接头角焊缝进行非熔化极惰性气体保护电弧焊(TIG)熔修,研究了熔修距离(热源中心至焊趾的距离,2,1,0,−1 mm)和熔修电流(150,170,190,210 A)对熔修后焊趾形状和接头疲劳性能的影响。结果表明:在熔修电流150 A条件下,当熔修距离为0时,熔修焊缝完全覆盖原始焊趾,焊趾曲率半径较大,母材与焊缝过渡平缓;当熔修距离为2,1 mm时,原始焊趾无法得到熔修;当熔修距离为−1 mm时,熔修焊缝中形成凹陷。在熔修距离为0条件下,不同电流下熔修后焊趾的曲率半径均大于原始焊趾,过渡角均低于原始焊趾,随着熔修电流的增加,曲率半径先减后增再减,过渡角先增后降,150 A熔修电流下的曲率半径最大,过渡角最小;170, 190, 210 A熔修电流下熔修接头的疲劳裂纹源位置由原始焊趾变为熔修焊缝和熔修熔合区,150 A熔修电流下接头未发生疲劳开裂;熔修后接头的疲劳寿命高于原始接头,且随着熔修电流的增加,接头的疲劳寿命先降后升再降,150 A熔修电流下接头的疲劳寿命最高。

关键词: TIG熔修;角焊缝;十字接头;疲劳性能;曲率半径;过渡角
中图分类号: TG444　　**文献标志码:** A　　**文章编号:** 1000-3738(2025)06-0063-06

0 引　言

工程机械领域的加强筋板、复杂框架等高强钢焊接结构常采用角焊缝接头[1-4]。与对接焊缝相比,角焊缝的几何形状更为灵活,其焊趾处的形状突变和组织突变会加剧应力集中,导致构件更易于发生疲劳开裂。因此,有必要选取合适的焊趾修整工艺及参数来有效提升角焊缝接头的强度和服役时间[5-7]。

目前,提高角焊缝接头疲劳强度和寿命的方法主要包括非熔化极惰性气体保护电弧焊(TIG)熔修、机加打磨、冲击强化和焊后热处理等[8-11]。与其他方法相比,TIG熔修具有工艺简单、操作方便、成本低、效果显著等优点[12]。在TIG熔修时TIG焊炬将焊趾处的焊缝金属重新熔化,以消除熔渣、楔块、咬边等焊接缺陷,改善焊趾外形,使焊缝与母材之间形成平滑过渡,从而减少应力集中,提高疲劳强度[13-14]。TIG熔修工艺参数包括电弧电压、熔修电流、熔修距离(热源中心至焊趾的距离)、焊枪倾斜角度、预热温度、焊接速度、气体流量等。IIW标准中对电弧电压、焊枪倾斜角度、预热温度、焊接速度、气体流量等参数作出了明确规定[15],但是未对熔修距离和熔修电流作出规定。因此,作者以工程机械常用Q690D低合金高强钢熔化极气体保护电弧焊(GMAW)十字接头为研究对象,在不同熔修距离和熔修电流下采用TIG熔修工艺对十字接头角焊缝进行熔修,研究了熔修距离和电流对角焊缝焊趾形状以及接头疲劳性能的影响,以期为填补熔修技术标准空白,指导Q690D高强钢接头工艺优化提供试验参考。

1 试样制备与试验方法

试验材料为16 mm厚的Q690D低合金高强钢板。采用GMAW对钢板进行焊接,接头形式为十字接头,2块腹板开45°坡口,焊接材料采用直径为1.4 mm的ER76-G铁基焊丝,化学成分(质量分数/%)为0.06~0.15C,1.40~1.85Mn,0.80~1.10Si,≤0.025P,≤0.025S,0.20~0.30Cr,1.40~1.80Ni,0.25~0.45Mo。GMAW打底焊的工艺参数为电弧电压27 V、焊接电流350 A、焊接速度350 mm·min^{-1};填充及盖面焊工艺参数为电弧电压28 V、焊接电

收稿日期: 2024-07-23;**修订日期:** 2025-02-28
作者简介: 白海明(1986—),男,河南商丘人,高级工程师,硕士
通信作者: 安洪亮高级工程师

流400 A、焊接速度350 mm·min^{-1}、层道间温度60～200 ℃。采用TIG熔修工艺对十字接头角焊缝进行熔修，根据IIW标准确定的工艺参数为电弧电压12～15 V、焊接速度100 mm·min^{-1}、气体流量12 L·min^{-1}、焊枪倾斜角度10°、预热温度60 ℃[15]。采用参数解耦方法设计试验：固定熔修电流为150 A，设置熔修距离为2，1，0，−1 mm[15]，通过观察焊趾的宏观形貌获得最优的熔修距离；在最优熔修距离下，将熔修电流设置为150，170，190，210 A，研究焊趾处的组织以及接头的疲劳性能。

在熔修后的十字接头横截面上截取金相试样，经打磨、抛光后，利用OLYMPUS SZ61TR型体视显微镜观察角焊缝焊趾处的宏观形貌。对十字接头角焊缝焊趾的曲率半径R与过渡角θ（如图1所示）进行测量，过渡角为焊趾处母材与焊缝夹角的补角，测4次取平均值。由于目前曲率半径无标准化的定义或公认的确定程序，根据文献[4，16]提出的忽略焊缝过渡几何偏差方法，贴近熔修焊趾进行三点画弧以确定曲率半径。采用$FeCl_3$饱和溶液将抛光后的金相试样腐蚀10 s后，采用OLYMPUS GX51型光学显微镜观察熔修焊缝的显微组织。在原始接头和熔修接头上截取如图2所示的疲劳试样，采用QBG-500H型疲劳试验机进行拉-拉疲劳试验，最大应力为300 MPa，加载频率为100 Hz，应力比为0.23，疲劳试验终止条件为试样断裂或循环次数达10^7周次，相同条件下测3次取平均值。

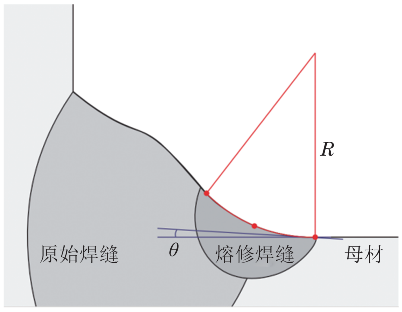

图1 角焊缝焊趾曲率半径和过渡角示意

Fig. 1 Schematic of curvature radius and transition angle of weld toe of fillet welds

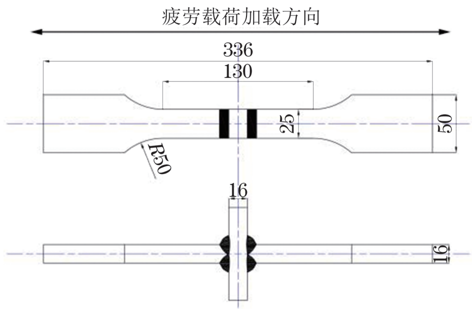

图2 疲劳试样的形状和尺寸

Fig. 2 Shape and dimension of fatigue specimen

2 试验结果与讨论

2.1 熔修距离对焊趾形状的影响

由图3可以看出：当熔修距离为2，1 mm时，原

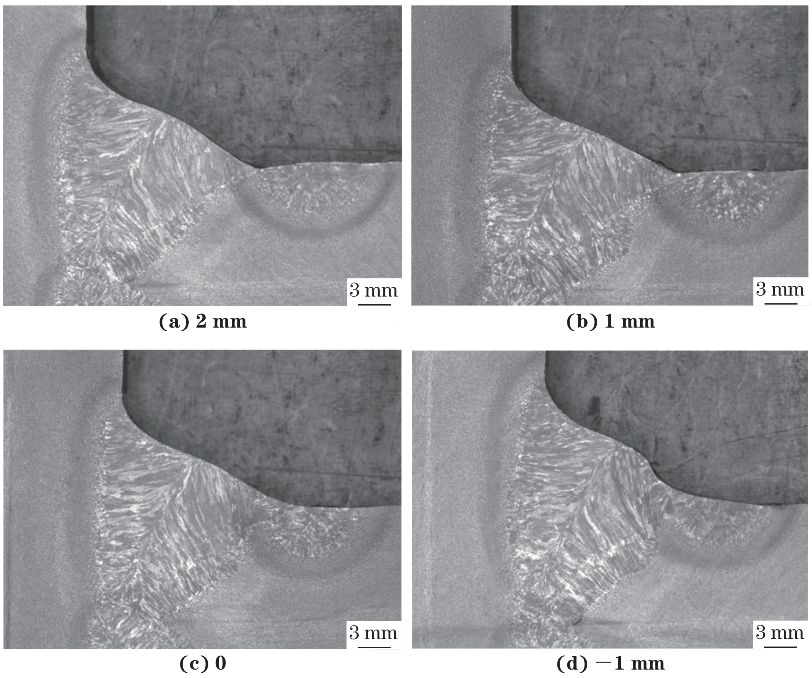

(a) 2 mm (b) 1 mm (c) 0 (d) −1 mm

图3 不同熔修距离下熔修角焊缝焊趾处的宏观组织（熔修电流150 A）

Fig. 3 Macrostructure of weld toe in remelted fillet welds under different remelting distances (remelting current of 150 A)

始接头焊趾处未发生重熔，该熔修工艺无法起到修缮焊趾形状的作用；当熔修距离为－1 mm时，熔修焊缝中形成明显的凹陷，凹陷位置易产生应力集中，降低其承载能力[17]；当熔修距离为0时，熔修焊缝完全覆盖原始焊趾，且曲率半径较大，母材与焊缝过渡平缓。因此，采用熔修效果最佳的熔修距离0对十字接头角焊缝进行TIG熔修。

2.2 熔修电流对焊趾形状和焊缝组织的影响

由图4可以看出：不同电流熔修后焊趾的曲率半径均大于原始接头焊趾，并且随着熔修电流的增加，焊趾的曲率半径先减后增再减，150 A熔修电流下的曲率半径最大，且测试值的离散程度低于其他熔修电流下；熔修后焊趾的过渡角低于原始焊趾，随着熔修电流增加，过渡角先增后降，150 A熔修电流下的过渡角最小，不同熔修电流下过渡角的离散程度差异不大。由图5可以看出：原始接头焊缝显微组织为贝氏体＋针状铁素体；当熔修电流为150，170，190 A时，除贝氏体和针状铁素体外，熔修焊缝中还存在少量马氏体，这是由于上述电流下的热输入低，冷却速率快，使得焊缝内生成了少量马氏体；当熔修电流为210 A时，熔修焊缝的显微组织为贝氏体＋针状铁素体，未观察到马氏体，这可能是由于热输入升高造成的。综上可知，熔修电流对焊趾表面形状和焊缝组织均会产生影响。

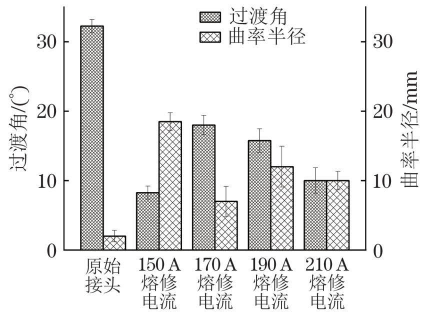

图4 原始接头焊趾和不同电流熔修焊趾的曲率半径和过渡角

Fig. 4 Curvature radius and transition angle of original joint weld toe and remelted weld toe under different remelting currents

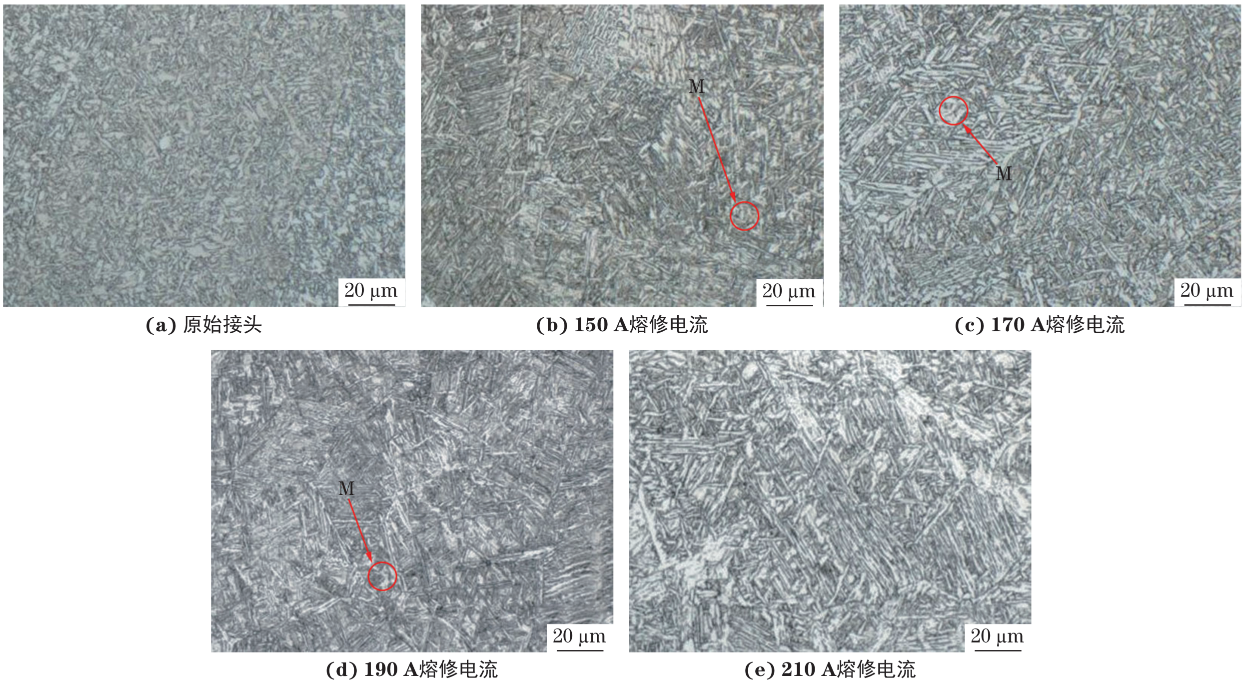

(a) 原始接头 (b) 150 A熔修电流 (c) 170 A熔修电流 (d) 190 A熔修电流 (e) 210 A熔修电流

图5 原始接头焊缝和不同电流熔修焊缝的显微组织

Fig. 5 Microstructures of original joint weld (a) and remelted weld under different remelting currents (b–e)

2.3 熔修电流对接头疲劳性能的影响

由图6(a)可以看出：熔修后接头的疲劳寿命高于原始接头。随着熔修电流的增加，熔修后接头的疲劳寿命先降后升再降，150 A熔修电流下接头的疲劳寿命最高，循环10^7周次后试样均未断裂；当熔修电流为170，190，210 A时，熔修后接头的疲劳寿命与原始接头相比分别约提高2.4，8.6，5.8倍。结合焊趾形状参数可知，熔修接头的疲劳性能与熔修焊趾的曲率半径呈正相关，与过渡角基本呈负相关，这与文献[18]中角焊缝接头疲劳寿命的主要影响因素为焊趾曲率半径和过渡角相吻合。由图6和表1可以看出，原始接头均在焊趾处断裂，这是由于形状因素导致原始焊趾处应力集中，疲劳裂纹于焊趾处萌生；经170，190，210 A电流熔修后疲劳裂纹源位于熔修

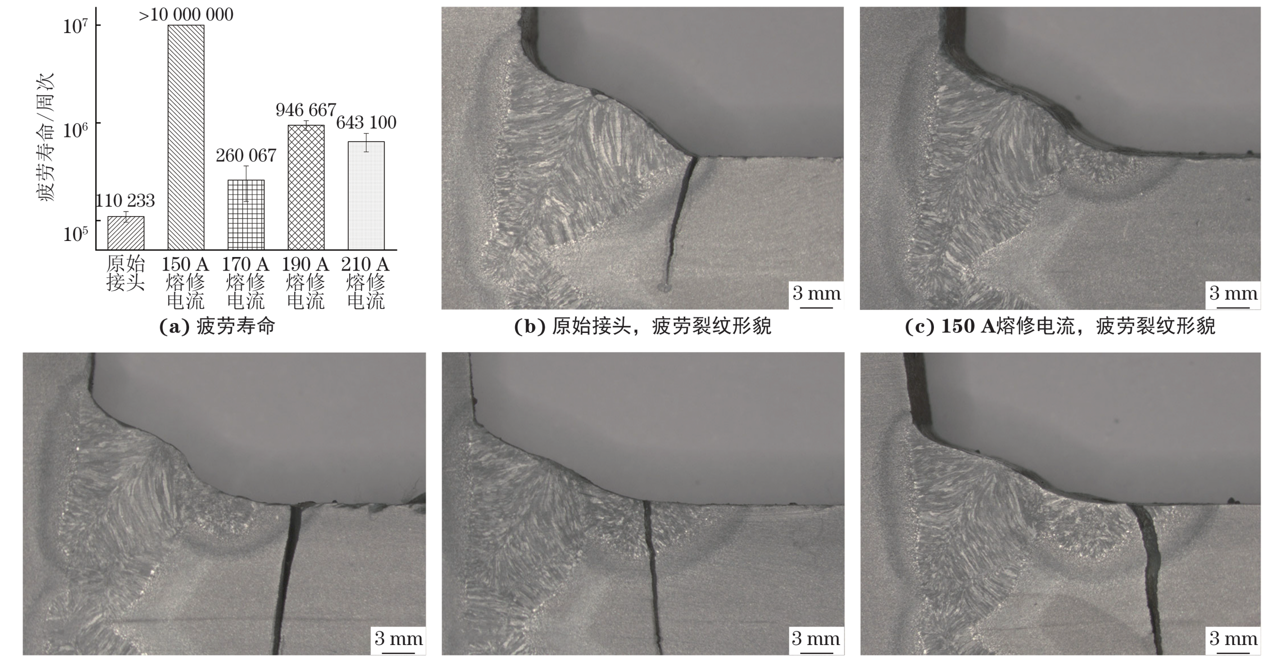

(a) 疲劳寿命 (b) 原始接头，疲劳裂纹形貌 (c) 150 A熔修电流，疲劳裂纹形貌

(d) 170 A熔修电流，疲劳裂纹形貌 (e) 190 A熔修电流，疲劳裂纹形貌 (f) 210 A熔修电流，疲劳裂纹形貌

图6　原始接头和不同电流熔修接头的疲劳寿命以及典型疲劳裂纹形貌

Fig. 6　Fatigue life (a) and typical fatigue crack morphology (b–f) of original joint (b) and remelted joint under different remelting currents (c–f)

表1　原始接头和不同电流熔修接头中不同位置疲劳裂纹源数量统计

Table 1　Count statistics of fatigue crack sources at different positions in original joint and remelted joint under different remelting currents

条件	不同位置疲劳裂纹源数量/个		
	原始接头焊趾	熔修焊缝	熔修熔合区
原始接头	3		
150 A熔修电流		0	0
170 A熔修电流		1	2
190 A熔修电流		2	1
210 A熔修电流		2	1

焊缝和熔修熔合区，这是因为TIG熔修有效缓解了原始接头焊趾处的应力集中程度。

3　结　论

（1）当熔修距离为0时，TIG熔修焊缝完全覆盖原始十字接头焊趾，焊趾曲率半径较大，母材与焊缝过渡平缓；当熔修距离为2，1 mm时，原始焊缝焊趾无法得到熔修；当熔修距离为−1 mm时，熔修焊缝中形成凹陷。

（2）在熔修距离为0条件下，不同电流熔修后焊趾的曲率半径均大于原始焊趾，随着熔修电流的增加，曲率半径先减后增再减，150 A熔修电流下的曲率半径最大；焊趾的过渡角均低于原始焊趾，随着熔修电流的增加，过渡角先增后降，150 A熔修电流下的过渡角最小。

（3）170，190，210 A熔修电流下熔修接头的疲劳裂纹源位置由原始接头的焊趾变为熔修焊缝和熔修熔合区，150 A熔修电流下接头未发生疲劳开裂。熔修后接头的疲劳寿命高于原始接头，且随着熔修电流的增加，熔修接头的疲劳寿命先降后升再降，150 A熔修电流下的疲劳寿命最高，循环10^7周次后试样均未断裂；熔修接头的疲劳性能与焊趾曲率半径呈正相关，与过渡角基本呈负相关。

参考文献：

[1]　邢红云，郭良权，倪梁华，等. 5083/6061异种铝合金角焊缝组织与性能分析[J]. 热加工工艺，2019，48(1)：185-188.
XING H Y，GUO L Q，NI L H，et al. Microstructure and performance analysis of 5083/6061 dissimilar Al alloy fillet weld[J]. Hot Working Technology，2019，48(1)：185-188.

[2]　吴智峰. 焊接速度对45钢/N80钢异种材料螺旋角焊缝组织与硬度影响研究[J]. 热加工工艺，2018，47(5)：190-193.
WU Z F. Effect of welding speed on microstructure and hardness of spiral welding seam of 45 steel/N80 steel dissimilar materials[J]. Hot Working Technology，2018，47(5)：190-193.

[3] 张立平,张立杰,袁晓明,等.基于静力等承载强度的T型接头角焊缝焊脚尺寸确定及疲劳特性[J].电焊机,2023,53(11):96-100.
ZHANG L P,ZHANG L J,YUAN X M,et al. Determination of weld leg size and fatigue characteristics of T-joint fillet welds based on static equal bearing strength[J]. Electric Welding Machine, 2023, 53(11): 96-100.
[4] 范志东,张志博,马翼超,等.超超临界锅炉水冷壁吹灰器密封盒角焊缝开裂的原因[J].机械工程材料,2019,43(12):77-82.
FAN Z D, ZHANG Z B, MA Y C, et al. Reason for cracking of fillet weld between water wall and soot blower seal box in an ultra-supercritical boiler[J]. Materials for Mechanical Engineering, 2019, 43(12): 77-82.
[5] 张军,张凤梅,周韶泽.惯性载荷作用下结构应力法焊接结构抗疲劳性能研究[J].大连交通大学学报,2019,40(1):40-45.
ZHANG J, ZHANG F M, ZHOU S Z. Study on fatigue performance of weld structure under inertial loading using structure stress method[J]. Journal of Dalian Jiaotong University, 2019, 40(1): 40-45.
[6] ANDUD D, SAIDIN S, MANURUNG Y H P. Fatigue life behaviour of transverse fillet weld and transverse fillet on weld of the HSLA S460G2+M followed by HFMI/PIT[J]. Applied Mechanics and Materials, 2020, 899: 126-134.
[7] 钟广生,魏国前,闫梦煜,等.焊趾半径对疲劳短裂纹演化行为的影响[J].焊接学报,2023,44(11):88-95,133-134.
ZHONG G S, WEI G Q, YAN M Y, et al. Study on the influence of weld toe radius on the evolution behavior of fatigue short cracks[J]. Transactions of the China Welding Institution, 2023, 44(11): 88-95, 133-134.
[8] 李亚杰,刘涛,洪磊,等. 不同焊丝TIG焊SUS316L/15CrMo异种钢接头的显微组织与力学性能[J].机械工程材料,2023,47(10):43-49.
LI Y J, LIU T, HONG L, et al. Microstructure and mechanical properties of SUS316L/15CrMo dissimilar steel joint by TIG welding with different welding wires[J]. Materials for Mechanical Engineering, 2023, 47(10): 43-49.
[9] 何柏林,张枝森,谢学涛,等.超声冲击和机械打磨提高SMA490BW钢焊接接头超高周疲劳性能[J].中国铁道科学,2017,38(5):107-113.
HE B L, ZHANG Z S, XIE X T, et al. Very high cycle fatigue performance improvement of SMA490BW steel welded joint by ultrasonic impact and mechanical polishing treatment[J]. China Railway Science, 2017, 38(5): 107-113.
[10] 徐国建,钟立明,杭争翔,等.铝合金焊接接头冲击强化的性能[J].焊接学报,2014,35(6):57-60.
XU G J, ZHONG L M, HANG Z X, et al. Performance of shock processing on aluminum alloy welded joint[J]. Transactions of the China Welding Institution, 2014, 35(6): 57-60.
[11] 李季涛,兆文忠,田长亮.焊后热处理退火工艺对十字接头疲劳寿命的影响[J].金属热处理,2020,45(9):86-90.
LI J T, ZHAO W Z, TIAN C L. Influence of post-weld annealing process on fatigue life of cross joint[J]. Heat Treatment of Metals, 2020, 45(9): 86-90.
[12] FERRO P, ROMANIN L. An efficient model for the TIG-dressing process numerical simulation[J]. Material Design & Processing Communications, 2019, 1(3): e35.
[13] HAAGENSEN P J, MADDOX S J. IIW recommendations on methods for improving the fatigue strength of welded joints[M]. Cambridge: Woodhead Publishing Limited, 2013.
[14] WU L C, WANG D P. Improve the fatigue performance of welded joints with undercuts by TIG dressing treatment[J]. Advanced Materials Research, 2012, 472/473/474/475: 1300-1304.
[15] HOBBACHER A F. The new IIW recommendations for fatigue assessment of welded joints and components: A comprehensive code recently updated[J]. International Journal of Fatigue, 2009, 31(1): 50-58.
[16] ZERBST U, MADIA M, VORMWALD M. Fatigue strength and fracture mechanics[J]. Procedia Structural Integrity, 2017, 5: 745-752.
[17] 李畅.考虑几何尺寸效应的T型接头疲劳性能研究[D].重庆:重庆交通大学,2024.
LI C. Study on the fatigue properties of T-joints considering geometric size effect[D]. Chongqing: Chongqing Jiaotong University, 2024.
[18] 王立君.焊缝几何对焊趾疲劳裂纹扩展行为的影响[J].天津大学学报,1997,30(6):735-740.
WANG L J. Influences of weld geometry on behavior of fatigue crack growth at weld toes[J]. Journal of Tianjin University (Science and Technology), 1997, 30(6): 735-740.

Effect of TIG Remelting Distance and Current on Fatigue Performance of Q690D Steel GMAW Cross Joints

BAI Haiming[1], LI Zihao[2], MA Yiming[2], AN Hongliang[2]

(1. Zhengzhou Coal Mining Machinery Group Co., Ltd., Zhengzhou 450016, China;
2. Harbin Welding Institute Limited Company, Harbin 150028, China)

Abstract: The fillet weld of the gas metal arc welding (GMAW) cross joint of Q690D low alloy high strength steel was remelted by non-melting inert gas shielded arc welding (TIG). The effects of the remelting distance (distance from the center of the heat source to the weld toe, 2, 1, 0, −1 mm) and the remelting current (150, 170, 190, 210 A) on the shape of the weld toe after remelting and the fatigue performance of the joints were studied. The results show that under the remelting current of 150 A, when the remelting distance was 0, the remelted weld completely covered the original weld toe, the curvature radius of the weld toe was large, and the transition between the base metal and the weld was smooth. When the remelting distances were 2 mm and 1 mm, the original weld toe could not be remelted. When the remelting distance was −1 mm, a depression was formed in the remelted weld. Under the remelting distance of 0, the curvature radius of the weld toe after remelting under different currents was larger than that of the original weld toe, and the transition angle was lower than that of the original weld toe. With the increase of the remelting current, the curvature radius first decreased, then increased, and then decreased, while the transition angle first increased and then decreased. The curvature radius was the largest and the transition angle was the smallest at the remelting current of 150 A. Under the remelting currents of 170, 190, 210 A, the fatigue crack source positions of the remelted joints changed from the original weld toe to the remelted weld and the remelted fusion zone. No fatigue cracking occurred in the joint under the remelting current of 150 A. The fatigue life of the joint after remelting was higher than that of the original joint. With the increase of the remelting current, the fatigue life of the remelted joint first decreased, then increased, and then decreased again, and was the highest at the remelting current of 150 A.

Key words: TIG remelting; fillet weld; cross joint; fatigue property; curvature radius; transition angle

（上接第62页）

Effect of Cryogenic Treatment on Milling Machined Surface Quality of DC53 Steel

LI Min

(Intelligent Manufacturing Key Laboratory of Luzhou City, College of Intelligent Manufacturing and Automotive Engineering, Luzhou Vocational and Technical College, Luzhou 646100, China)

Abstract: The DC53 steel after conventional heat treatment was subjected to cryogenic treatment in the −196 ℃ liquid nitrogen for different time periods (3, 6, 9 h). End milling and side milling were carried out by using cemented carbide end mills. The effects of cryogenic treatment on the microstructure and milling machined surface quality of the test steel were studied. The results show that the tempered martensite and retained austenite in the DC53 steel were refined after cryogenic treatment. The amount of fine granular carbides increased and dispersed in the matrix. With the extension of cryogenic treatment time, the grain refinement effect became more obvious, the amount of fine granular carbides increased, and the microstructure became more uniform. When the cryogenic treatment time was extended to 9 h, the size of some granular carbides increased. After cryogenic treatment, the number and depth of grooves or furrows on the milling machined surface decreased, and the surface roughness was reduced. As the cryogenic treatment time extended, the number and depth of grooves or furrows first decreased and then slightly increased, and the surface roughness also first decreased and then slightly increased. After cryogenic treatment for 6 h, the milling machined surface roughness was the lowest, and compared with those before cryogenic treatment, the surface roughness of end milling and side milling machined surfaces decreased by 25.8% and 21.6%, respectively; the surface quality was the best.

Key words: DC53 steel; cryogenic treatment; milling machining; surface roughness